JOURNAL OF COMPUTATIONAL PHYSICS **145,** 166–192 (1998)
ARTICLE NO. CP986028

A Diffusion-Generated Approach to Multiphase Motion

Steven J. Ruuth[1]

Department of Mathematics, University of California, 405 Hilgard Avenue, Los Angeles, California 90095-1555
E-mail: ruuth@math.ucla.edu

Received July 2, 1997; revised May 8, 1998

In this article, we present a diffusion-generated approach for evolving multiple junctions. This work generalizes an earlier method by Merriman, Bence, and Osher which alternately diffuses and sharpens characteristic functions for each phase region to produce pure mean curvature flow. Specifically, our new method produces a normal velocity which depends on a positive multiple of the curvature of the interface plus the difference in bulk energy densities for prescribed junction angles. This simple method naturally treats topological mergings and breakings, produces no overlapping regions or vacuums, and can be made very fast. Numerical studies are provided which show that our method agrees with front tracking and a recent variational approach for a variety of examples. Asymptotic expansions are also carried out near junctions to justify our algorithms.

1. INTRODUCTION

In a variety of applications, one wants to follow the motion of a front that moves with some curvature-dependent speed. For the special case of pure mean curvature flow, junctions of moving surfaces have been treated by alternately diffusing and sharpening the characteristic functions for each phase region [9, 10]. In this work, we generalize this diffusion-generated approach to allow each interface to move with a normal velocity equal to a positive multiple of its curvature, κ, plus a constant.

In two dimensions, the simplest model that we consider involves three curves meeting at a point with prescribed angles θ_1, θ_2, and θ_3. Each interface, Γ_{ij}, separates regions Ω_i and

[1] This research was partially supported by an NSERC Postdoctoral Scholarship, ONR N00014-97-1-0027 and NSF DMS94-04942.

0021-9991/98 $25.00

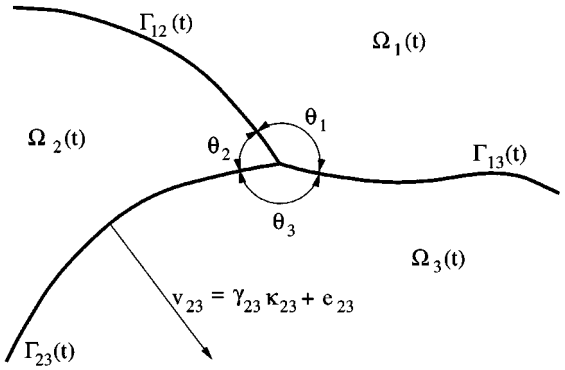

FIG. 1. The interfaces, Γ_{ij}, move with a normal velocity $v_{ij} = \gamma_{ij}\kappa_{ij} + e_{ij}$ and are subject to angles $\theta_1, \theta_2, \theta_3$.

Ω_j and moves with a normal velocity,

$$v_{ij} = \gamma_{ij}\kappa_{ij} + e_{ij} \tag{1}$$

as is shown in Fig. 1.

A simple motivation for this model is obtained by associating an energy functional with the system [11, 18]: Given r distinct regions, we set the total energy of the system equal to the interface energy

$$E_{interface} = \sum_{1 \le i < j \le r} f_{ij}\ \text{Length}(\Gamma_{ij})$$

plus the bulk energy

$$E_{bulk} = \sum_{i=1}^{r} b_i\ \text{Area}(\Omega_i),$$

where f_{ij} is the constant surface tension of Γ_{ij} and b_i is the (constant) bulk energy density for Ω_i. The corresponding gradient flow is then given by

$$v_{ij} = \mu_{ij}(f_{ij}\kappa_{ij} + b_i - b_j), \tag{2}$$

where κ_{ij} and μ_{ij} denote, respectively, the local curvature and the constant mobility of the interface Γ_{ij} [11]. The velocity of the model (1) is then obtained by setting $\gamma_{ij} = \mu_{ij} f_{ij}$ and $e_{ij} = \mu_{ij}(b_i - b_j)$ in Eq. (2) above. See [1, 3, 11, 17, 18] for further details on the model and its derivation.

To numerically approximate motions of the form (1), several methods have been developed. Front tracking methods (e.g., [4]) are often well-suited for curves that never cross because they explicitly approximate the motion of the interface rather than a level set of some higher dimensional function. When line or planar segments interact, however, decisions must be made as to whether to insert or delete segments. Because complicated topological changes can occur for the model problem (1) implementation of front tracking methods is often impractical, especially for more than two dimensions.

Other approaches also have limitations. Monte-Carlo methods for Potts models can introduce unwanted anisotropy into the motion due to the spatial mesh [17] and are typically

too slow to find accurate approximations of the model. Phase field methods may also be used, but these are often inherently too expensive for practical computation [10] because they represent the interface as an internal layer, and thus require an extremely fine mesh (at least locally) to resolve this layer.

To address these concerns for the case of pure mean curvature flow (i.e., each $\gamma_{ij} = 1$ and $e_{ij} = 0$), a method (MBO) based on alternatively diffusing and sharpening characteristic functions was proposed by Merriman, Bence, and Osher [9, 10]. This method naturally handles complicated topological changes with junctions in several dimensions. Furthermore, this method can be made efficient by discretizing in space using a Fourier spectral basis and using a quadrature to determine the Fourier coefficients at each step [13, 14]. Similarly to all other methods for multiple phase problems, no convergence results are known for the MBO-method. However, [6, 2] do give rigorous convergence proofs for two phase mean curvature motion and [8, 13] give some further asymptotic results.

To allow for the more general motion (1), a variational approach was recently proposed [18] which gives a practical method for treating junctions even when topological mergings and breakings occur. This interesting approach is especially well-suited for treating problems with additional constraints. Unfortunately, it is unable to approximate many problems involving $r > 3$ phase regions since only r independent γ_{ij} or e_{ij} may be prescribed Furthermore, this method limits angles to the classical condition (see, e.g., [16])

$$\frac{\sin(\theta_1)}{\gamma_{23}} = \frac{\sin(\theta_2)}{\gamma_{13}} = \frac{\sin(\theta_3)}{\gamma_{12}} \tag{3}$$

at triple points and is relatively slow when compared to the MBO-method for the case of pure mean curvature flow.

In this paper, we develop algorithms for the multiphase model (1) for any number of phase regions which retain the speed and much of the simplicity of the MBO-method. Although the methods given throughout this paper are semi-discrete, we note that efficient[2] implementations are possible using the algorithms described in [13, 14]. An outline of the paper follows.

In Section 2, we give the MBO-method for two phase and multiple phase problems.

Section 3 generalizes the MBO-method to nonsymmetric junctions by replacing the sharpening step with a new decision. Asymptotic and numerical justifications of our algorithm are also given.

In Section 4, we diffuse each characteristic function a number of times (once for each γ_{ij}) and combine the results with the nonsymmetric junction algorithm. This gives a method for evolving each branch with a normal speed $v = \gamma_{ij}\kappa$ for prescribed angle conditions. For the special (but important) case where the angles obey the classical condition (3), asymptotic and numerical justifications of our algorithms are given.

By changing the sharpening decision, Sections 5 and 6 extend these methods to models which involve bulk energies and any number of phase regions. Numerical justifications of our methods are given and an example of a four-phase problem which cannot be treated using the variational approach is also provided.

Section 7 concludes by summarizing our results and discussing some possible areas of future research.

[2] Using a step size Δt, $\mathcal{O}((1/\Delta t)\log(\Delta t))$ operations are needed for each step of the algorithm [13, 14].

2. THE MBO-METHOD

An algorithm for following interfaces propagating with a normal velocity equal to mean curvature was introduced by Merriman, Bence, and Osher [9, 10]. In this section, we describe the method for the two phase and multiple phase problems. Subsequent sections describe new algorithms which generalize these methods to the multiphase motions described by Eq. (1).

2.1. *The Two Phase Problem*

Suppose we wish to follow an interface moving with a normal velocity equal to its mean curvature. To evolve a surface according to this motion, we may use the MBO-method for two regions:

MBO-Method (*Two Regions*).

BEGIN

(1) Set U equal to the characteristic function for the initial region.

i.e., set $U(\mathbf{x}, 0) = \begin{cases} 1 & \text{if } \mathbf{x} \text{ belongs to the initial region} \\ 0 & \text{otherwise.} \end{cases}$

REPEAT for all steps, j, from 1 to the final step:

BEGIN

(2) Apply diffusion[3] to U for some time, Δt.

i.e., find $U(\mathbf{x}, j\Delta t)$ using $\begin{cases} U_t = \nabla^2 U, \\ \frac{\partial U}{\partial n} = 0 \qquad \text{on } \partial\mathcal{D} \end{cases}$

starting from $U(\mathbf{x}, (j-1)\Delta t)$.

(3) "Sharpen" the diffused region by setting

$U(\mathbf{x}, j\Delta t) = \begin{cases} 1 & \text{if } U(\mathbf{x}, j\Delta t) > \frac{1}{2} \\ 0 & \text{otherwise.} \end{cases}$

END

END

For any time t, the level set $\{\mathbf{x} : U(\mathbf{x}, t) = \frac{1}{2}\}$ gives the location of the interface.

An extension to the case where the normal velocity equals the mean curvature plus a constant,

$$v_n = a + \kappa$$

is also possible. This motion can be obtained by following the level set

$$\frac{1}{2} - \frac{1}{2} a \sqrt{\frac{\Delta t}{\pi}} \tag{4}$$

instead of the usual level set of $\frac{1}{2}$ [8].

[3] Here we have selected zero flux boundary conditions to ensure that the curve meets the boundary at right angles, as is appropriate for certain grain growth models [4]. Alternatively, one may minimize the effects of the boundary by selecting non-reflecting boundary conditions, $\frac{\partial^2 U}{\partial n^2} = 0$, (cf. [18]) or use Dirichlet conditions to produce a constrained motion.

2.2. *Multiple Regions*

To obtain a normal velocity equal to the mean curvature for symmetric junctions (e.g., a 120–120–120 degree junction in two dimensions), we may apply the MBO-method for multiple regions:

MBO-Method (*Multiple* (r) *Regions*).

BEGIN

(1) For $i = 1, \ldots, r$

Set $U_i(\mathbf{x}, 0)$ equal to the characteristic function for the ith region.

REPEAT for all steps, j, from 1 to the final step:

BEGIN

(2) For $i = 1, \ldots, r$, starting from $U_i(\mathbf{x}, (j-1)\Delta t)$,

Apply diffusion to U_i for some time slice, Δt.

i.e., find $U_i(\mathbf{x}, j\Delta t)$ using $\begin{cases} \frac{\partial U_i}{\partial t} = \nabla^2 U_i, \\ \frac{\partial U_i}{\partial n} = 0 \qquad \text{on } \partial\mathcal{D}. \end{cases}$

(3) "Sharpen" the diffused regions by setting the largest U_i equal to 1 and the others equal to 0 for each point on the domain.

END

END

For any time t, the interfaces are given naturally as the boundaries of the characteristic sets.

3. NONSYMMETRIC JUNCTIONS

The MBO-method for regions uses a symmetric projection step which results in an approximation of a 120-120-120 degree junction. We now extend the method to allow for nonsymmetric junctions and justify our algorithm asymptotically and experimentally.

Throughout the next three sections, we will consider the three phase case. See Section 6 for an extension to more phase regions.

3.1. *Nonsymmetric Junction Algorithm*

We now generalize the sharpening step for the MBO-method to obtain an algorithm for nonsymmetric junctions.

Begin by noting that

$$0 \le U_i(\mathbf{x}, t) \le 1,$$

$$\sum_{i=1}^{3} U_i(\mathbf{x}, t) = 1$$

for all t since diffusion in linear and $\sum_{i=1}^{3} U_i(\mathbf{x}, 0) = 1$. Thus, the ordered triplets, (U_1, U_2, U_3), form a triangular region with corners (0, 0, 1), (0, 1, 0), and (1, 0, 0) in $\Re^3$. By mapping this triangular region onto its corner points we obtain a useful representation of

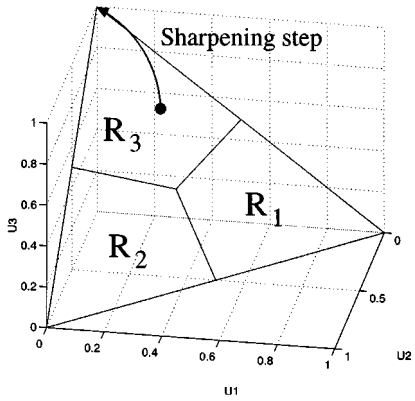

FIG. 2. The sharpening decision can be represented using a projection triangle. For the symmetric case, the regions R_1, R_2, and R_3 meet at straight lines which pass through $(\frac{1}{3}, \frac{1}{3}, \frac{1}{3})$ and the midpoints of the edges of the triangular domain.

the sharpening step [8, 10]. For example, the symmetric sharpening is obtained by setting

$$(U_1, U_2, U_3) = \begin{cases} (0,0,1) & \text{if } (U_1, U_2, U_3) \in R_1 \\ (0,1,0) & \text{if } (U_1, U_2, U_3) \in R_2 \\ (1,0,0) & \text{if } (U_1, U_2, U_3) \in R_3, \end{cases}$$

where R_1, R_2, and R_3 divide the triangular domain symmetrically, as shown in Fig. 2. Other, nonsymmetric, angle configurations are obtained by taking different choices for R_1, R_2, and R_3.

We now develop a method for determining R_1, R_2, and R_3 for curves which meet at a stable θ_1-θ_2-θ_3 angle configuration. To derive this method we note that in the absence of boundary effects (cf. [8]),

> straight lines which form a junction satisfying the desired angle conditions must remain stationary for all subsequent times, t (e.g., Fig. 3).

By enforcing this simple, but necessary condition we are led to the following algorithm for constructing projection triangles:

Initial Regions, $t = 0$ Later Regions, $t > 0$

FIG. 3. Straight lines forming θ_1-θ_2-θ_3 angles should remain stationary.

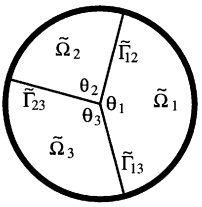

FIG. 4. Initial regions.

PROJECTION TRIANGLE ALGORITHM.

Given an angle configuration $\theta_1, \theta_2, \theta_3$:

1. Define lines

$$\tilde{\Gamma}_{12} = \left\{ \left(r, \frac{1}{2}\theta_1 \right) : r > 0 \right\},$$
$$\tilde{\Gamma}_{13} = \left\{ \left(r, -\frac{1}{2}\theta_1 \right) : r > 0 \right\},$$
$$\tilde{\Gamma}_{23} = \left\{ \left(r, \frac{1}{2}\theta_1 + \theta_2 \right) : r > 0 \right\}$$

   and regions, $\tilde{\Omega}_1, \tilde{\Omega}_2, \tilde{\Omega}_3$ as indicated by Fig. 4. Here, a circular domain has been selected for simplicity.
2. Set χ_i equal to the characteristic function for $\tilde{\Omega}_i$, $1 \le i \le 3$, as shown in Fig. 5.
3. Apply diffusion to each χ_i, $1 \le i \le 3$, for a time $\tau \le \Delta t$ as is illustrated in Fig. 6.
4. Map each line $\tilde{\Gamma}_{ij}$ onto the projection triangle to form the boundaries, $\tilde{\tilde{\Gamma}}_{ij}$ between regions R_i and R_j,

$$\tilde{\tilde{\Gamma}}_{ij} = \{(\chi_1(\mathbf{x}), \chi_2(\mathbf{x}), \chi_3(\mathbf{x})) : \mathbf{x} \in \tilde{\Gamma}_{ij}\}$$

   as is illustrated[4] in Fig. 7. It is convenient to represent $\tilde{\tilde{\Gamma}}_{ij}$ in polar coordinates centered about the junction (see Fig. 8). Using this representation it is straightforward to determine which region a point $P = (r_p, \theta_p)$ belongs since

$$P \in \begin{cases} R_1 & \text{if } \theta_{12}(r_p) \le \theta_p \text{ or } \theta_p < \theta_{13}(r_p) \\ R_2 & \text{if } \theta_{23}(r_p) \le \theta_p < \theta_{12}(r_p) \\ R_3 & \text{if } \theta_{13}(r_p) \le \theta_p < \theta_{23}(r_p). \end{cases}$$

Having constructed our projection triangle, it is straightforward to derive the following properties [8]:

- Each boundary curve passes through $(\frac{\theta_1}{2\pi}, \frac{\theta_2}{2\pi}, \frac{\theta_3}{2\pi})$.
- Each curve must also meet the midpoint of an edge of the triangular domain since this case reduces to the MBO-algorithm for two phases.

[4] On non-circular domains, only half of each line $\tilde{\Gamma}_{ij}$ should be mapped (starting from the junction). By connecting this result to the midpoint of the nearest edge of the projection triangle, an excellent approximation of $\tilde{\tilde{\Gamma}}_{ij}$ is formed, provided τ is sufficiently small.

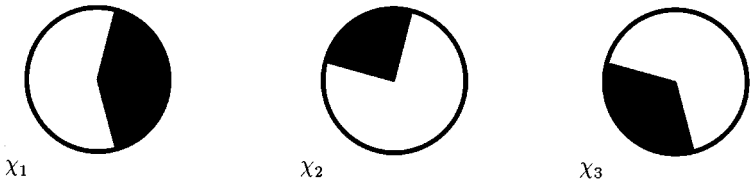

FIG. 5. Characteristic sets.

Note, however, that the lines connecting these endpoints are typically curved. This is quite clearly illustrated for a 150–90–120 degree junction in Fig. 9 and for a wedge-shaped junction in Fig. 10. In fact, only the symmetric case and the 180–90–90 degree "T-Junction" are comprised of straight lines (see Fig. 11).

3.2. *Error Analysis*

In the previous subsection, we proposed an algorithm for evolving junctions which meet at a stable θ_1–θ_2–θ_3 angle configuration. We now outline a derivation that shows, symbolically (using Maple [5]), that each step of the method produces an $\mathcal{O}(\sqrt{\Delta t})$ error in the junction angles which is rapidly dissipated in subsequent steps.

Due to the length of the expressions arising in our derivation, we provide the main steps of the algorithm, but omit most of the intermediate results. See [13] for greater details for the special case of a symmetric junction.

3.2.1. The initial junction. We wish to derive an expansion for the angles of a two dimensional triple junction after one step of our method assuming that the angles initially approximate the desired θ_1–θ_2–θ_3 configuration.

We begin by orienting a polar coordinate system so that some phase region is centered about $\theta = 0$. Denote the initial interfaces by Γ_{12}, Γ_{13}, and Γ_{23} and the initial regions by Ω_1, Ω_2, and Ω_3 as in Fig. 12.

To represent the small deviations from the θ_1–θ_2–θ_3 junction configuration we define

$$\begin{aligned}\epsilon_1 &= \angle\Gamma_{13}\Gamma_{12} - \theta_1,\\ \epsilon_2 &= \angle\Gamma_{12}\Gamma_{23} - \theta_2,\\ \epsilon_3 &= \angle\Gamma_{13}\Gamma_{23} - \theta_3,\end{aligned}$$

where $\angle\Gamma_{ij}\Gamma_{kl}$ is the angle between Γ_{ij} and Γ_{kl} at the junction.

In order to carry out our expansions, we want an expression for each interface,

$$\Gamma_{ij} = \left\{\left(r, \theta_{\Gamma_{ij}}(r)\right) : r \geq 0\right\}$$

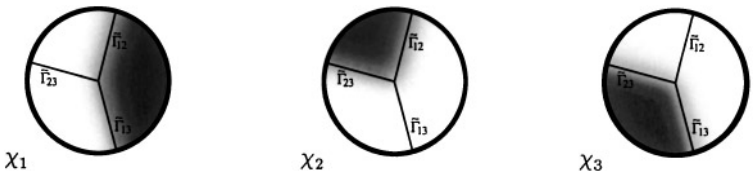

FIG. 6. After a time τ.

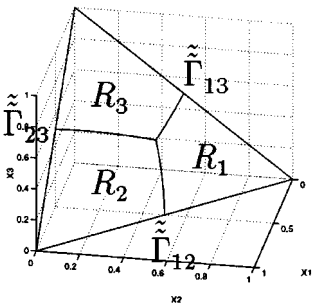

FIG. 7. Projection triangle formed by mapping $\tilde{\Gamma}_{ij}$ into $\chi_1 + \chi_2 + \chi_3 = 1$.

for some function, $\theta_{\Gamma_{ij}}(r)$. Using the above definitions it is straightforward to show that

$$\theta_{\Gamma_{12}}(r) = \frac{1}{2}\theta_1 + \frac{1}{2}\epsilon_1 + \frac{1}{2}\kappa_{12} r + \beta_{12} r^2 + \mathcal{O}(r^3),$$
$$\theta_{\Gamma_{23}}(r) = \frac{1}{2}\theta_1 + \theta_2 + \frac{1}{2}\epsilon_1 + \epsilon_2 + \frac{1}{2}\kappa_{23} r + \beta_{23} r^2 + \mathcal{O}(r^3),$$
$$\theta_{\Gamma_{13}}(r) = -\frac{1}{2}\theta_1 - \frac{1}{2}\epsilon_1 + \frac{1}{2}\kappa_{13} r + \beta_{13} r^2 + \mathcal{O}(r^3),$$

where κ_{ij} is the curvature of line Γ_{ij} at the origin and β_{ij} are constants independent of r.

3.2.2. Approximation of U_i and χ_i. We now want to estimate U_i at time Δt and χ_i at time, τ. Initially,

$$U_i(r, \theta, 0) = \begin{cases} 1 & \text{if } (r, \theta) \in \Omega_i \\ 0 & \text{otherwise,} \end{cases}$$

for $1 \le i \le 3$. Thus, the Green's function representation of $U_1(r, \theta, \Delta t)$ gives

$$U_1(r, \theta, \Delta t) = \frac{1}{4\pi \Delta t} \exp\left(-\frac{r^2}{4\Delta t}\right) \int_0^\infty \exp\left(-\frac{R^2}{4\Delta t}\right) \int_{\theta_{\Gamma_{13}}(R)}^{\theta_{\Gamma_{12}}(R)} \exp\left(\frac{r R \cos(\phi - \theta)}{2\Delta t}\right) R \, d\phi \, dR.$$

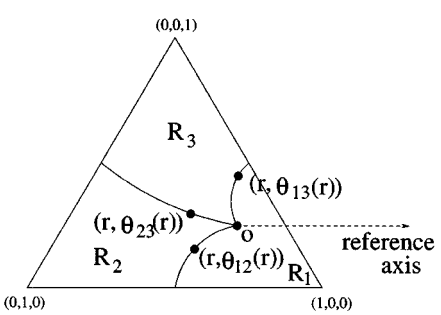

FIG. 8. The boundaries between regions are conveniently represented in polar coordinates centered about the junction.

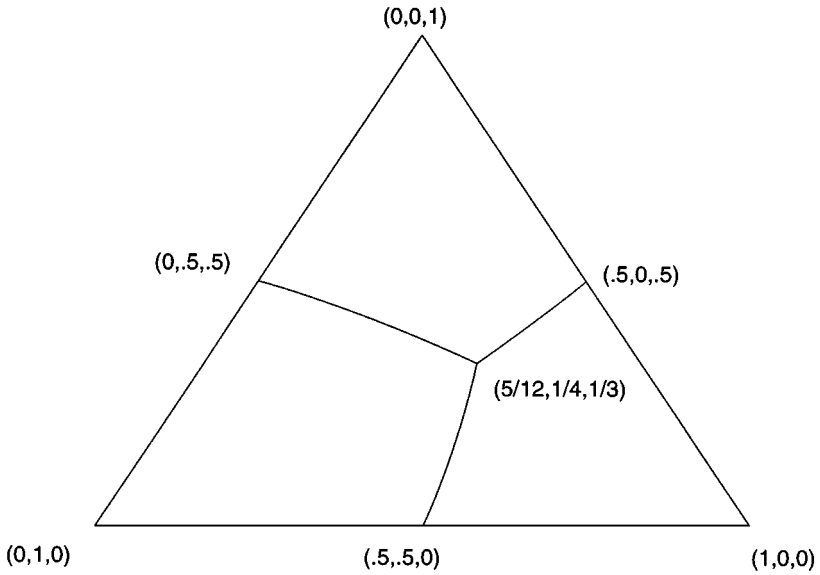

FIG. 9. The projection triangle for a 150–90–120 degree junction.

Replacing the exponential in the inner integral by its series, integrating term by term, and applying integration by parts to the result (cf. [8, 13]) yields

$$\begin{aligned} U_1(r,\theta,\Delta t) = {} & \frac{\theta_1}{2\pi} + \frac{1}{2\pi}\epsilon_1 + \frac{1}{4\sqrt{\pi}}(\kappa_{12}-\kappa_{13})\sqrt{\Delta t} + \frac{2}{\pi}(\beta_{12}-\beta_{13})\Delta t \\ & + \frac{1}{2\pi}(\kappa_{12}-\kappa_{13})\cos(\theta_1)\cos(\theta)\, r + \frac{1}{2\pi}(\kappa_{12}+\kappa_{13})\sin(\theta_1)\sin(\theta)\, r \\ & + \frac{1}{2\sqrt{\pi}}\sin(\theta_1)\cos(\theta)\left(\frac{r}{\sqrt{\Delta t}}\right) + \frac{1}{2\sqrt{\pi}}\cos(\theta_1)\cos(\theta)\,\epsilon_1\left(\frac{r}{\sqrt{\Delta t}}\right) \\ & + \frac{1}{4\pi}\sin(\theta_1)\cos(\theta_1)(\cos^2(\theta)-\sin^2(\theta))\left(\frac{r}{\Delta t}\right)^2 + \text{h.o.t.} \end{aligned}$$

which may be written in Cartesian coordinates as

$$\begin{aligned} U_1(x,y,\Delta t) = {} & \frac{\theta_1}{2\pi} + \frac{1}{2\pi}\epsilon_1 + \frac{1}{4\sqrt{\pi}}(\kappa_{12}-\kappa_{13})\sqrt{\Delta t} + \frac{2}{\pi}(\beta_{12}-\beta_{13})\Delta t \\ & + \frac{1}{2\pi}(\kappa_{12}-\kappa_{13})\cos(\theta_1)\, x + \frac{1}{2\pi}(\kappa_{12}+\kappa_{13})\sin(\theta_1)\, y \\ & + \frac{1}{2\sqrt{\pi}}\sin(\theta_1)\left(\frac{x}{\sqrt{\Delta t}}\right) + \frac{1}{2\sqrt{\pi}}\cos(\theta_1)\,\epsilon_1\left(\frac{x}{\sqrt{\Delta t}}\right) \\ & + \frac{1}{4\pi}\sin(\theta_1)\cos(\theta_1)\left(\frac{x^2-y^2}{(\Delta t)^2}\right) + \text{h.o.t.} \end{aligned} \tag{5}$$

To determine an expansion for the value of χ_1 which arises in the Projection Triangle Algorithm, simply set

$$\epsilon_1 = \epsilon_2 = \epsilon_3 = 0,$$
$$\kappa_{12} = \kappa_{23} = \kappa_{13} = 0,$$
$$\beta_{12} = \beta_{23} = \beta_{13} = 0$$

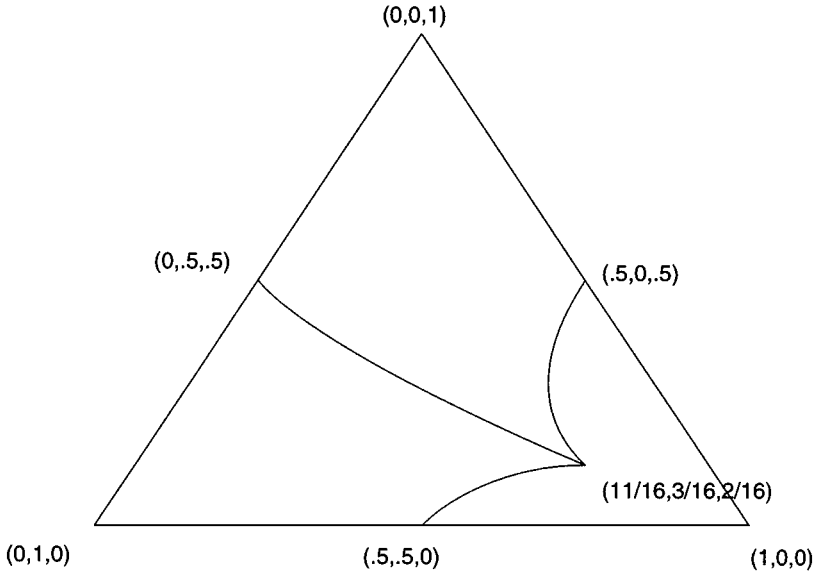

FIG. 10. The projection triangle for a 247.5–67.5–45 degree junction.

in Eq. (5) to obtain

$$\chi_1(x, y, \tau) = \frac{\theta_1}{2\pi} + \frac{1}{2\sqrt{\pi}} \sin(\theta_1)\left(\frac{x}{\sqrt{\tau}}\right) + \frac{1}{4\pi} \sin(\theta_1)\cos(\theta_1)\left(\frac{x^2 - y^2}{\tau^2}\right) + \text{h.o.t.} \quad (6)$$

Expressions for the remaining U_i and χ_i are easily obtained via rotations of Eqs. (5) and (6), respectively.

3.2.3. Angle expansions. We now seek expansions for the angle configuration of the junction after a time Δt.

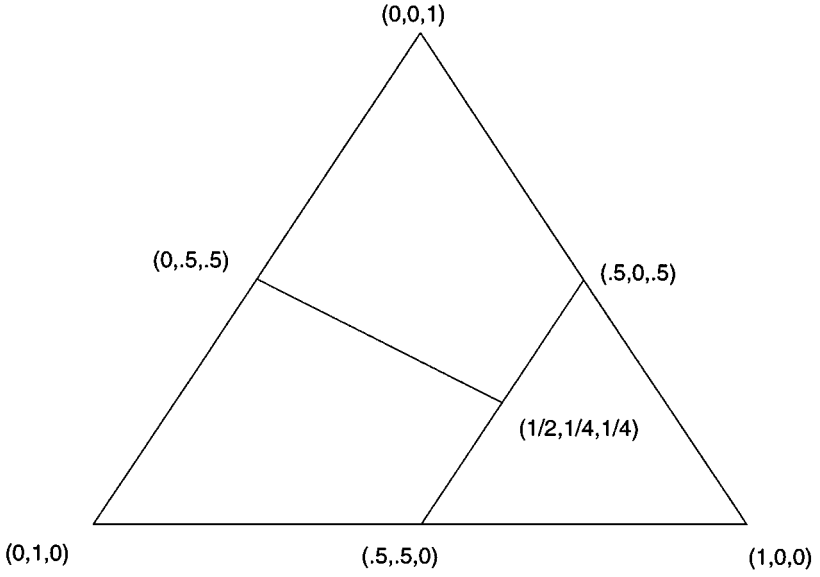

FIG. 11. The projection triangle for a 180–90–90 degree junction.

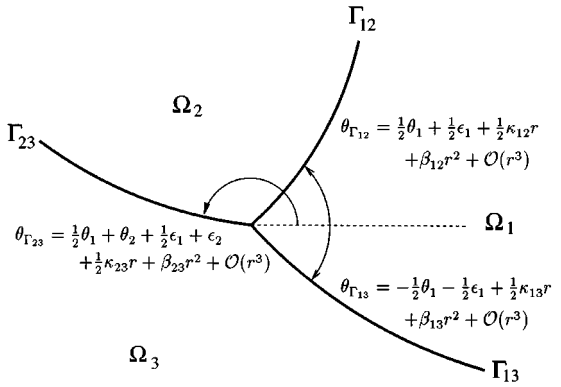

FIG. 12. The initial junction.

Begin by letting $\Gamma_{12}^{\Delta t}$, $\Gamma_{23}^{\Delta t}$, and $\Gamma_{13}^{\Delta t}$ be the diffusion-generated approximations to the branches of the junction after a time Δt and parameterize the components of $\Gamma_{ij}^{\Delta t}$ according to

$$\Gamma_{ij}^{\Delta t} = \left\{ \left(x_{\Gamma_{ij}^{\Delta t}}(s), y_{\Gamma_{ij}^{\Delta t}}(s) \right) : s \geq 0 \right\},$$

where s represents arclength from the triple point. Similarly define the components of each branch, $\tilde{\Gamma}_{ij}$, of the stationary problem according to

$$\tilde{\Gamma}_{ij} = \left\{ \left(x_{\tilde{\Gamma}_{ij}}(s), y_{\tilde{\Gamma}_{ij}}(s) \right) : s \geq 0 \right\}.$$

To approximate the angle between $\Gamma_{12}^{\Delta t}$ and $\Gamma_{13}^{\Delta t}$ we require an expansion for the location of the triple point at time $t = \Delta t$. This is found by substituting our estimates for U_i into

$$\begin{cases} U_1\left(x_{\Gamma_{ij}^{\Delta t}}(0), y_{\Gamma_{ij}^{\Delta t}}(0), \Delta t \right) = \frac{1}{2\pi}\theta_1, \\ U_2\left(x_{\Gamma_{ij}^{\Delta t}}(0), y_{\Gamma_{ij}^{\Delta t}}(0), \Delta t \right) = \frac{1}{2\pi}\theta_2 \end{cases}$$

and deriving the series solution for $(x_{\Gamma_{ij}^{\Delta t}}(0), y_{\Gamma_{ij}^{\Delta t}}(0))$.

Our next task is to find the slope of $\Gamma_{ij}^{\Delta t}$ at the triple point. This is accomplished by substituting our expressions for U_i and χ_i into

$$\frac{d}{ds}\left[U_i\left(x_{\Gamma_{ij}^{\Delta t}}(s), y_{\Gamma_{ij}^{\Delta t}}(s), \Delta t \right) \right]_{s=0} = \frac{d}{ds}\left[\chi_i\left(x_{\tilde{\Gamma}_{ij}}(s), y_{\tilde{\Gamma}_{ij}}(s), \tau \right) \right]_{s=0}$$
$$\frac{d}{ds}\left[U_j\left(x_{\Gamma_{ij}^{\Delta t}}(s), y_{\Gamma_{ij}^{\Delta t}}(s), \Delta t \right) \right]_{s=0} = \frac{d}{ds}\left[\chi_j\left(x_{\tilde{\Gamma}_{ij}}(s), y_{\tilde{\Gamma}_{ij}}(s), \tau \right) \right]_{s=0},$$

where

$$\left(x_{\tilde{\Gamma}_{ij}}(0), y_{\tilde{\Gamma}_{ij}}(0) \right) = (0, 0),$$
$$\left(x'_{\tilde{\Gamma}_{12}}(0), y'_{\tilde{\Gamma}_{12}}(0) \right) = \left(\cos\left(\frac{1}{2}\theta_1\right), \sin\left(\frac{1}{2}\theta_1\right) \right),$$
$$\left(x'_{\tilde{\Gamma}_{13}}(0), y'_{\tilde{\Gamma}_{13}}(0) \right) = \left(\cos\left(\frac{1}{2}\theta_1\right), -\sin\left(\frac{1}{2}\theta_1\right) \right),$$
$$\left(x'_{\tilde{\Gamma}_{23}}(0), y'_{\tilde{\Gamma}_{23}}(0) \right) = \left(\cos\left(\frac{1}{2}\theta_1 + \theta_2\right), \sin\left(\frac{1}{2}\theta_1 + \theta_2\right) \right)$$

and deriving series solutions for $x'_{\Gamma_{ij}^{\Delta t}}(0)$ and $y'_{\Gamma_{ij}^{\Delta t}}(0)$. These expansions give the slope of $\Gamma_{ij}^{\Delta t}$ at the triple point,

$$m_{ij} = \frac{y'_{\Gamma_{ij}^{\Delta t}}(0)}{x'_{\Gamma_{ij}^{\Delta t}}(0)}.$$

From the slopes of each branch, we see that the approximation to the first angle, θ_1, is given by

$$\angle \Gamma_{12}^{\Delta t} \Gamma_{13}^{\Delta t} = \pi - \arctan\left(\frac{m_{12} - m_{13}}{1 + m_{12} m_{13}}\right).$$

Expanding this in terms of ϵ_i and Δt gives

$$\angle \Gamma_{12}^{\Delta t} \Gamma_{13}^{\Delta t} = \theta_1 + a_{11}\epsilon_1 + a_{12}\epsilon_2 + (c_{11}\kappa_{12} + c_{12}\kappa_{23} + c_{13}\kappa_{13})\sqrt{\Delta t} + \text{h.o.t.}$$

A similar derivation gives the approximation for the second angle, θ_2,

$$\angle \Gamma_{23}^{\Delta t} \Gamma_{12}^{\Delta t} = \theta_2 + a_{21}\epsilon_1 + a_{22}\epsilon_2 + (c_{21}\kappa_{22} + c_{22}\kappa_{23} + c_{23}\kappa_{13})\sqrt{\Delta t} + \text{h.o.t.}$$

Combining these results into a single equation we obtain

$$\begin{pmatrix} \angle \Gamma_{12}^{\Delta t} \Gamma_{13}^{\Delta t} \\ \angle \Gamma_{23}^{\Delta t} \Gamma_{12}^{\Delta t} \end{pmatrix} = \begin{pmatrix} \theta_1 \\ \theta_2 \end{pmatrix} + A \begin{pmatrix} \epsilon_1 \\ \epsilon_2 \end{pmatrix} + C \begin{pmatrix} \kappa_{12} \\ \kappa_{23} \\ \kappa_{13} \end{pmatrix} \sqrt{\Delta t} + \text{h.o.t.},$$

where $A = [a_{ij}]$ and $C = [c_{ij}]$.

Unfortunately, the matrices A and C are far too complicated to reproduce here. However, we do provide a contour plot of the spectral radius of A for each angle configuration $(\theta_1, \theta_2, \theta_3)$ in Fig. 13a. This plot indicates that the spectral radius of A is always less than 1. Similarly, we find that each element of C is bounded in the interior of the triangle (see Fig. 13b). Thus, each step of the MBO-method produces an $\mathcal{O}(\sqrt{\Delta t})$ error in the junction angles which is rapidly dissipated during subsequent steps. Summing up such contributions[5] over many time steps, we expect to obtain a rapidly converging geometric sum which gives rise to an $\mathcal{O}(\sqrt{\Delta t})$ error in total. This is an interesting result because it gives an explanation for the stability of junction angles and suggests a source of the $\mathcal{O}(\sqrt{\Delta t})$ error which arises in numerical experiments (see the next subsection).

3.3. *Numerical Experiments*

We now apply our algorithm to problems involving nonsymmetric junctions. See also [8, 10] for experimental studies of the 180–90–90 degree "T-Junction" case.

To begin, consider the motion by curvature of the three phase problem given in Fig. 14. Using our nonsymmetric junction algorithm, the position of the triple point and the change

[5] This summation step is non-rigorous because it assumes, among other things, that κ_{12}, κ_{23}, and κ_{13} are bounded independent of Δt.

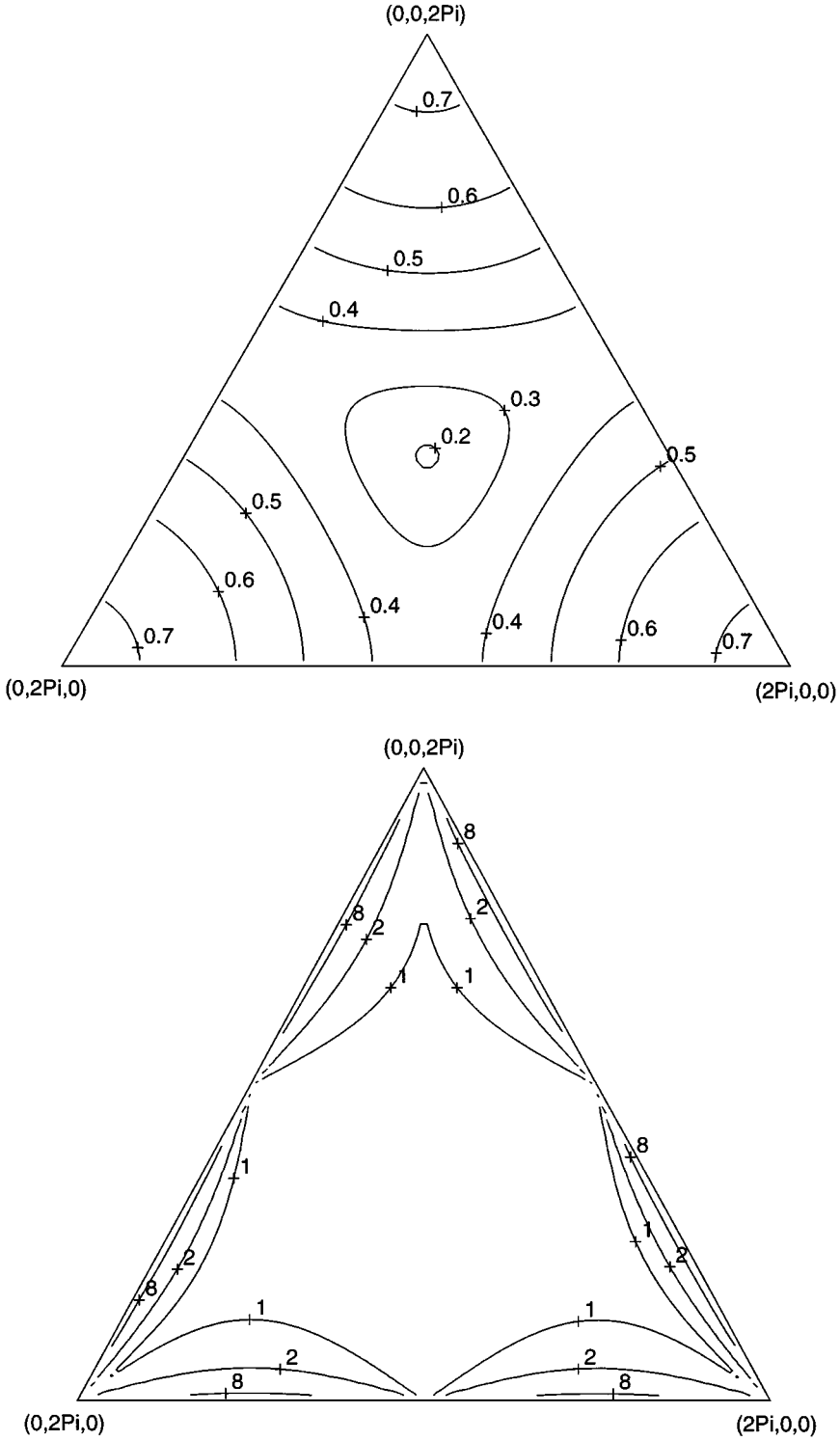

FIG. 13. Matrix properties for each angle configuration $(\theta_1, \theta_2, \theta_3)$. Note that $\theta_1+\theta_2+\theta_3 = 2\pi$ and each angle is between 0 and 2π so each configuration must belong to the triangular region with corners $(0, 0, 2\pi)$, $(0, 2\pi, 0)$, and $(2\pi, 0, 0)$ in $\mathcal{R}^3$. (a) The spectral radius of A. (b) The maximum element of $C = \max |c_{ij}|$.

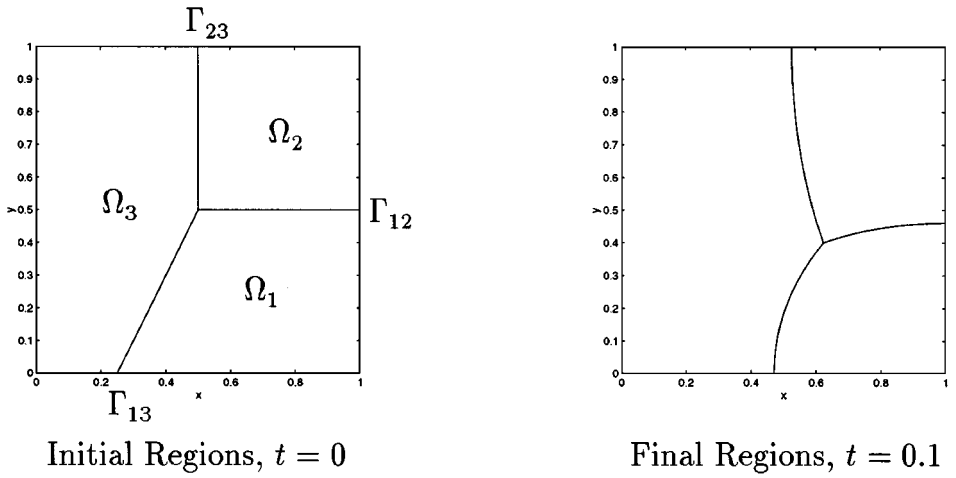

FIG. 14. A test problem for a 150–90–120 degree junction. Here, each $\gamma_{ij} = 1$ and each $e_{ij} = 0$.

in the area of Ω_1 were compared with the exact results[6] for several Δt. The results from a number of experiments are reported in Table I.

These results are suggestive of an $\mathcal{O}(\sqrt{\Delta t})$ error which is experimentally the same as that found for symmetric junctions using the MBO-method [13, 12, 14].

Our new algorithm can even be applied to wedge-shaped regions or to problems which are initially inconsistent with the desired angle configuration. Consider, for example, the motion by curvature of the three phase problem given in Fig. 15. Using our nonsymmetric junction algorithm, the position of the triple point and the change in the area of Ω_1 were compared with the exact results for several Δt. The results from a number of experiments are reported in Table II.

As found in the previous example, the results are suggestive of an $\mathcal{O}(\sqrt{\Delta t})$ error.

4. GENERALIZED CURVATURE MOTIONS

In the previous section, we described a method that treats nonsymmetric junctions for the case of pure curvature flow. We now extend the algorithm to the case where each branch, Γ_{ij}, moves with a normal speed, $v_n = \gamma_{ij}\kappa$.

Although the algorithm that we provide applies to any angle configuration, our asymptotic justification and numerical experiments will assume (for simplicity) the classical condition (3) at triple points which is well known in the material sciences literature (see, e.g., [16]).

4.1. *Generalized Curvature Algorithm*

We now generalize diffusion-generated motion to the case where each Γ_{ij} moves with a normal velocity,

$$v_n = \gamma_{ij}\kappa. \tag{7}$$

[6] The "exact results" were computed using Brian Wetton's front tracking code. See [4].

TABLE I
Results for a 150–90–120 Degree Junction

	Junction position		Phase area change for Ω_1	
Δt	*|Error|*	*Conv. rate*[a]	*|Error|*	*Conv. rate*
0.01	5.23e-03	—	3.80e-03	—
0.005	4.03e-03	0.38	2.55e-03	0.58
0.0025	3.05e-03	0.41	1.75e-03	0.54
0.00125	2.25e-03	0.43	1.20e-03	0.54
0.000625	1.65e-03	0.45	8.35e-04	0.52
0.0003125	1.20e-03	0.46	5.86e-04	0.51

[a] If the error for a step of size Δt is $E_{\Delta t}$, then we estimate the convergence rate as $\log_2(|E_{2\Delta t}/E_{\Delta t}|)$.

To begin, let $U_k^{\gamma_{ij}}$ be the solution to $u_t = \gamma_{ij}\nabla^2 u$ after a time Δt, starting from the characteristic function of Ω_k and set $\mathbf{U}^{\gamma_{ij}} = (U_1^{\gamma_{ij}}, U_2^{\gamma_{ij}}, U_3^{\gamma_{ij}})$. We seek a function, f, which combines $\mathbf{U}^{\gamma_{12}}$, $\mathbf{U}^{\gamma_{23}}$, and $\mathbf{U}^{\gamma_{13}}$ into a single result

$$\mathbf{U} \equiv (U_1, U_2, U_3) = f(\mathbf{U}^{\gamma_{12}}, \mathbf{U}^{\gamma_{23}}, \mathbf{U}^{\gamma_{13}})$$

which can be input to the sharpening step.

Several desirable properties for f are easily identified:

- Certainly, $f(\mathbf{U}^{\gamma_{12}}, \mathbf{U}^{\gamma_{23}}, \mathbf{U}^{\gamma_{13}})$ must reduce to the appropriate $\mathbf{U}^{\gamma_{ij}}$ far from the triple point. Specifically,

$$f(\mathbf{U}^{\gamma_{12}}, \mathbf{U}^{\gamma_{23}}, \mathbf{U}^{\gamma_{13}}) \approx \mathbf{U}^{\gamma_{ij}}$$

for all points near Γ_{ij} which are a distance $d \gg \sqrt{\Delta t}$ away from the triple point.

- We want f to be a smooth combination of the $\mathbf{U}^{\gamma_{ij}}$ so that the interfaces corresponding to $\mathbf{U}$ are smooth.

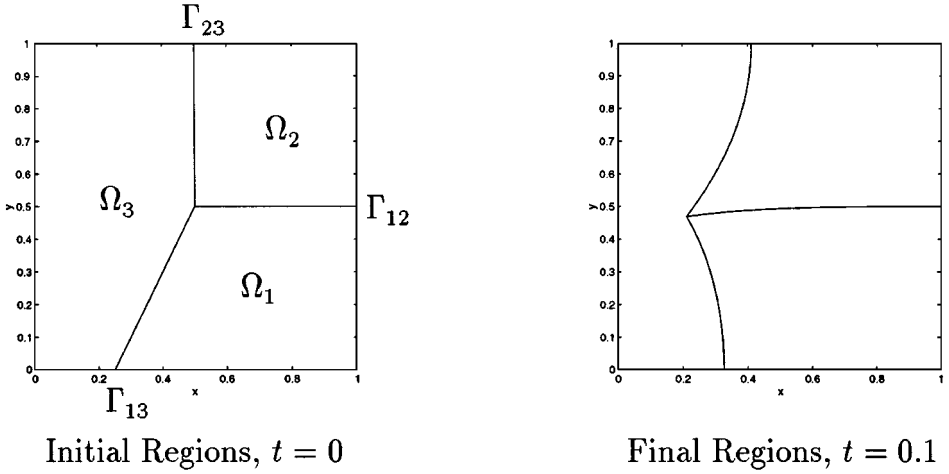

FIG. 15. A test problem for a 247.5–67.5–45 degree junction. Here, each $\gamma_{ij} = 1$ and each $e_{ij} = 0$.

TABLE II
Results for a 247.5–67.5–45 Degree Junction

	Junction position		Phase area change for Ω_1	
Δt	$\lvert Error\rvert$	*Conv. rate*	$\lvert Error\rvert$	*Conv. rate*
0.01	2.65e-02	—	1.76e-02	—
0.005	2.48e-02	0.09	1.41e-02	0.33
0.0025	2.14e-02	0.22	1.09e-02	0.37
0.00125	1.73e-02	0.30	8.28e-03	0.40
0.000625	1.34e-02	0.37	6.16e-03	0.43
0.0003125	9.47e-03	0.51	4.30e-03	0.52

• We will also assume that $\mathbf{U}$ is a convex combination of $\mathbf{U}^{\gamma_{12}}$, $\mathbf{U}^{\gamma_{23}}$, and $\mathbf{U}^{\gamma_{13}}$. This requirement ensures that each component of $\mathbf{U}$ belongs to [0, 1] and that the components of $\mathbf{U}$ sum to 1.

One simple family of functions which satisfy these requirements is given by

$$f_n(\mathbf{U}^{\gamma_{12}}, \mathbf{U}^{\gamma_{23}}, \mathbf{U}^{\gamma_{13}}) = \frac{\mathbf{U}^{\gamma_{12}}/\left|U_3^{\gamma_{12}}\right|^n + \mathbf{U}^{\gamma_{23}}/\left|U_1^{\gamma_{23}}\right|^n + \mathbf{U}^{\gamma_{13}}/\left|U_2^{\gamma_{13}}\right|^n}{\sum_{i=1}^{3}\left(U_i^{\gamma_{12}}/\left|U_3^{\gamma_{12}}\right|^n\right) + U_i^{\gamma_{23}}/\left|U_1^{\gamma_{23}}\right|^n + U_i^{\gamma_{13}}/\left|U_2^{\gamma_{13}}\right|^n}. \quad (8)$$

The next two subsections justify this choice of f for the cases $n=1$ and $n=2$. Larger values of n were found to produce less accurate results on the test problems we tried.

We now summarize by giving the generalized curvature algorithm:

GENERALIZED CURVATURE ALGORITHM. Given an angle configuration $(\theta_1, \theta_2, \theta_3)$ and coefficients $(\gamma_{12}, \gamma_{23}, \gamma_{13})$:

BEGIN
(1) Construct a projection triangle according to the projection triangle algorithm.
(2) For $i = 1, \ldots, 3$
Set $U_i(\mathbf{x}, 0)$ equal to the characteristic function for the ith region.
REPEAT for all steps, j, from 1 to the final step:
BEGIN
(3) For each coefficient $\gamma = \gamma_{12}, \gamma_{23}, \gamma_{13}$ and each region $i = 1, 2, 3$,

$$\text{Find } U_i^{\gamma}(\mathbf{x}, j\Delta t) \text{ using } \begin{cases} \frac{\partial U_i^{\gamma}}{\partial t} = \gamma \nabla^2 U_i^{\gamma} \\ \frac{\partial U_i^{\gamma}}{\partial n} = 0 \qquad \text{on } \partial\mathcal{D} \end{cases}$$

$$\text{starting from } U_i^{\gamma}(\mathbf{x}, (j-1)\Delta t) = U_i(\mathbf{x}, (j-1)\Delta t).$$

(4) Set $\mathbf{U}(\mathbf{x}, j\Delta t) = f_n(\mathbf{U}^{\gamma_{12}}, \mathbf{U}^{\gamma_{23}}, \mathbf{U}^{\gamma_{13}})$ where f_n in given by Eq. (8).
(5) "Sharpen" $\mathbf{U} = (U_1, U_2, U_3)$ according to the projection triangle defined in step (1).
END
END

4.2. *Error Analysis*

In the previous subsection, we proposed an algorithm for evolving junctions with a normal velocity, $v_n = \gamma_{ij}\kappa$, for arbitrary angle configurations. We now give asymptotic estimates for the angles arising from this algorithm when the classical condition (3) holds.

Begin by letting $\Gamma_{12}^{\Delta t}$, $\Gamma_{23}^{\Delta t}$, and $\Gamma_{13}^{\Delta t}$ be the diffusion-generated approximations to the branches of the junction after a time Δt and let

$$\begin{aligned}\epsilon_1 &= \angle\Gamma_{13}\Gamma_{12} - \theta_1,\\ \epsilon_2 &= \angle\Gamma_{12}\Gamma_{23} - \theta_2,\\ \epsilon_3 &= \angle\Gamma_{13}\Gamma_{23} - \theta_3\end{aligned}$$

be the initial errors in each junction angle (see Fig. 12). As outlined in Subsection 3.2, it is straightforward (but tedious) to derive asymptotic estimates for the junction angles,

$$\begin{pmatrix}\angle\Gamma_{12}^{\Delta t}\Gamma_{13}^{\Delta t}\\ \angle\Gamma_{23}^{\Delta t}\Gamma_{12}^{\Delta t}\end{pmatrix} = \begin{pmatrix}\theta_1\\ \theta_2\end{pmatrix} + A\begin{pmatrix}\epsilon_1\\ \epsilon_2\end{pmatrix} + C\begin{pmatrix}\kappa_{12}\\ \kappa_{23}\\ \kappa_{13}\end{pmatrix}\sqrt{\Delta t} + \text{h.o.t.}$$

Unfortunately, the matrices A and C are far too complicated to reproduce here. However, Fig. 16 gives contour plots of the spectral radius of A for each angle configuration $(\theta_1, \theta_2, \theta_3)$ for the choices $f = f_1$ and $f = f_2$ (see Eq. (8)).

From these plots, it is clear than that the spectral radius is less than 1 (indeed, it is typically much less than 1) for most angle configurations. For example, the spectral radius is less than 1 whenever the following simple (but crude) bound holds:

$$\max(\theta_1, \theta_2, \theta_3) < \begin{cases}175.9 \text{ degrees} & \text{if } f = f_1\\ 173.5 \text{ degrees} & \text{if } f = f_2.\end{cases} \tag{9}$$

Furthermore, contour plots indicate that each element of C is bounded independent of Δt provided each $\gamma_{ij} > 0$. Thus, each step of the method produces an $\mathcal{O}(\sqrt{\Delta t})$ error in the junction angles which is rapidly dissipated during subsequent steps provided the spectral radius of A is less than 1 (e.g., whenever condition (9) holds). Similar to the case of the Nonsymmetric Junction Algorithm (see Subsection 3.2) this result explains the stability of junction angles and suggests a source of the $\mathcal{O}(\sqrt{\Delta t})$ error which arises in numerical experiments (see the next section).

4.3. *Numerical Experiments*

We now apply the Generalized Curvature Algorithm to the case where each branch of a junction moves with a different normal velocity, $v_n = \gamma_{ij}\kappa$.

For example, consider the evolution of the three phase problem given in Fig. 17. Using the Generalized Curvature Algorithm, the position of the triple point and the change in the area of Ω_1 were compared with the exact results (see Footnote 6) for several Δt. The results from a number of experiments are reported in Table III for $f = f_1$ and in Table IV for $f = f_2$.

These results are suggestive of an $\mathcal{O}(\sqrt{\Delta t})$ error which is experimentally the same as the found for pure motion by curvature.

Either $f = f_1$ or $f = f_2$ is adequate for a wide variety of problems (see the previous subsection). The choice $f = f_1$ has a slightly wider range of applicability (see Eq. (9)).

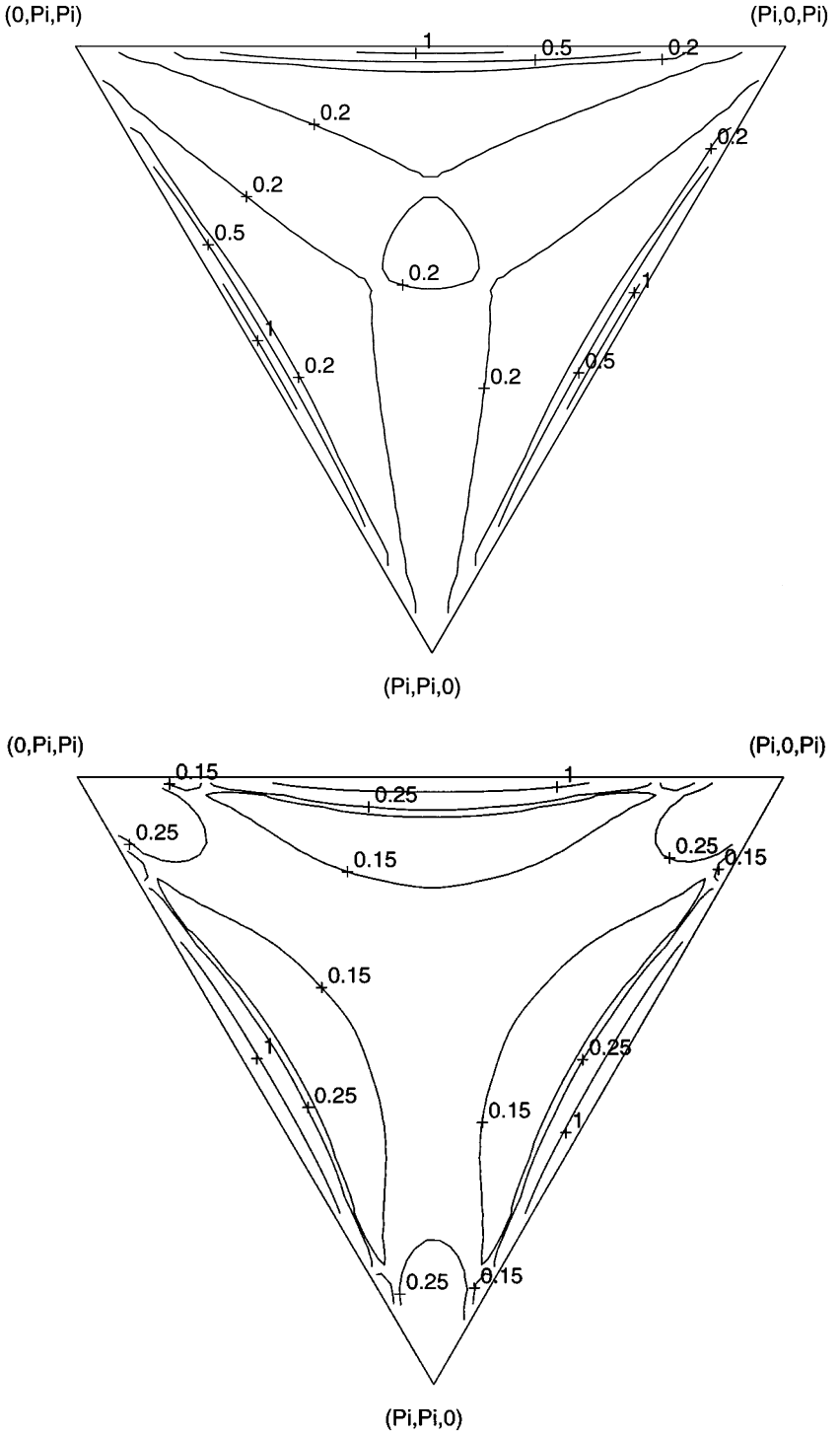

FIG. 16. The spectral radii arising for each angle configuration $(\theta_1, \theta_2, \theta_3)$. Here, the classical condition (3) restricts each angle to be between 0 and π, so each configuration must belong to the triangular region with corners $(0, 0, \pi)$, $(0, \pi, 0)$, and $(\pi, 0, 0)$. (a) Smoothest selection, $n = 1$. (b) Alternative choice, $n = 2$.

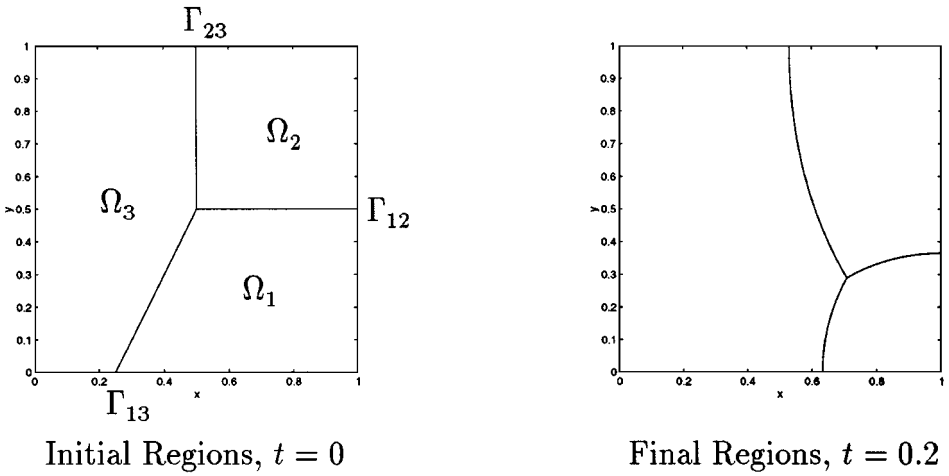

FIG. 17. A test problem for a 150–90–120 degree junction. Here, $(\gamma_{12}, \gamma_{23}, \gamma_{13}) = (\sin(\frac{5}{6}\pi), \sin(\frac{1}{2}\pi), \sin(\frac{2}{3}\pi))$ and each $e_{ij} = 0$.

The errors arising from $f = f_2$ are often more regular, however (e.g., compare Tables III and IV), which is a desirable property for determining an appropriate step size and for developing accurate, extrapolated algorithms [14].

5. MULTIPHASE MOTIONS

In the previous section we described a method to treat the case where each branch, Γ_{ij}, of a junction moves with a normal speed, $v_n = \gamma_{ij}\kappa$. We now extend the algorithm to allow more general multiphase motions which involve bulk energies (e.g., Fig. 1). Due to the complicated nature of the analysis, we justify our algorithms experimentally rather than asymptotically throughout the remainder of this article.

5.1. *Multiphase Motion Algorithm*

To carry out a sharpening appropriate for the multiphase model, we must construct new projection triangles. In particular, our projection triangles must satisfy the following:

(a) Along each edge, the sharpening decision must reduce to the case of two phase flow (4) since edges correspond to regions which are infinitely far from triple points [8].

TABLE III

Results for a 150–90–120 Degree Junction for $f = f_1$

	Junction position		Phase area change for Ω_1	
Δt	*|Error|*	*Conv. rate*	*|Error|*	*Conv. rate*
0.01	1.27e-02	—	1.97e-03	—
0.005	9.83e-03	0.37	1.76e-03	0.16
0.0025	7.37e-03	0.42	1.44e-03	0.29
0.00125	5.38e-03	0.45	1.12e-03	0.37
0.000625	3.83e-03	0.49	8.32e-04	0.43
0.0003125	2.67e-03	0.52	6.01e-04	0.47

TABLE IV
Results for a 150–90–120 Degree Junction for $f = f_2$

	Junction position		Phase area change for Ω_1	
Δt	$\lvert Error \rvert$	*Conv. rate*	$\lvert Error \rvert$	*Conv. rate*
0.01	1.03e-02	—	4.76e-03	—
0.005	7.41e-03	0.47	3.00e-03	0.66
0.0025	5.32e-03	0.48	1.96e-03	0.62
0.00125	3.79e-03	0.49	1.31e-03	0.58
0.000625	2.67e-03	0.50	8.94e-04	0.55
0.0003125	1.87e-03	0.51	6.12e-04	0.55

(b) In the limit $\Delta t \to 0$, the projection triangle must coincide with the case $(e_{12}, e_{13}, e_{23}) = (0, 0, 0)$ to obtain junction angles which are consistent with the desired configuration.

For the special case of symmetric junctions, these objectives are easily attained. We simply set each branch of the decision triangle to a straight line from $(\frac{1}{3}, \frac{1}{3}, \frac{1}{3})$ to the point dictated by Eq. (4). See Fig. 18 for an illustration of this construction.

For nonsymmetric junctions, appropriate projection triangles may be constructed by scaling and rotating the result of our original algorithm (see, e.g., Fig. 19) as follows:

PROJECTION TRIANGLE ALGORITHM FOR MULTIPHASE MOTION. Given an angle configuration $(\theta_1, \theta_2, \theta_3)$ and constants (e_{12}, e_{13}, e_{23}):

1. Construct a projection triangle using the algorithm given in Subsection 3.1. Represent the boundaries between the regions R_i and R_j of the triangle in polar coordinates, $\{(r, \theta_{ij}(r))\}$, as is shown in Fig. 8.

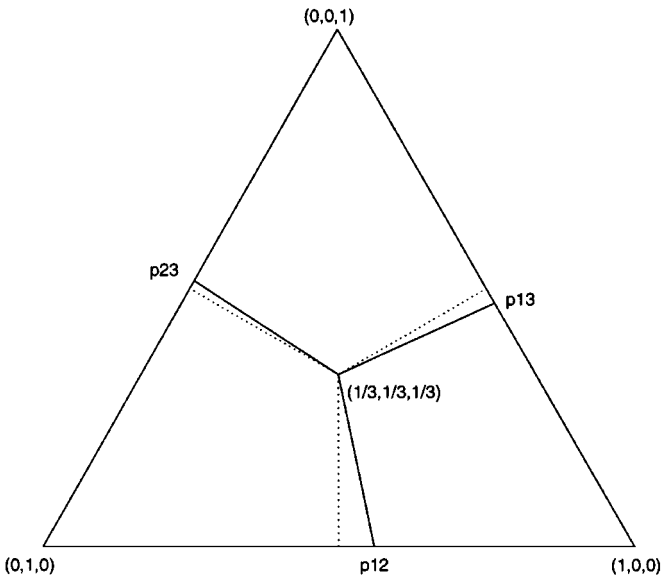

FIG. 18. The projection triangle for a 120–120–120 degree junction with (solid) and without (dotted) a constant component to the motion: $\mathbf{p}_{12} = (\frac{1}{2}+\frac{1}{2}e_{12}\sqrt{\frac{\Delta t}{2\pi}}, \frac{1}{2}-\frac{1}{2}e_{12}\sqrt{\frac{\Delta t}{2\pi}}, 0)$; $\mathbf{p}_{23} = (0, \frac{1}{2}+\frac{1}{2}e_{23}\sqrt{\frac{\Delta t}{2\pi}}, \frac{1}{2}-\frac{1}{2}e_{23}\sqrt{\frac{\Delta t}{2\pi}})$; $\mathbf{p}_{13} = (\frac{1}{2}+\frac{1}{2}e_{13}\sqrt{\frac{\Delta t}{2\pi}}, 0, \frac{1}{2}-\frac{1}{2}e_{13}\sqrt{\frac{\Delta t}{2\pi}})$.

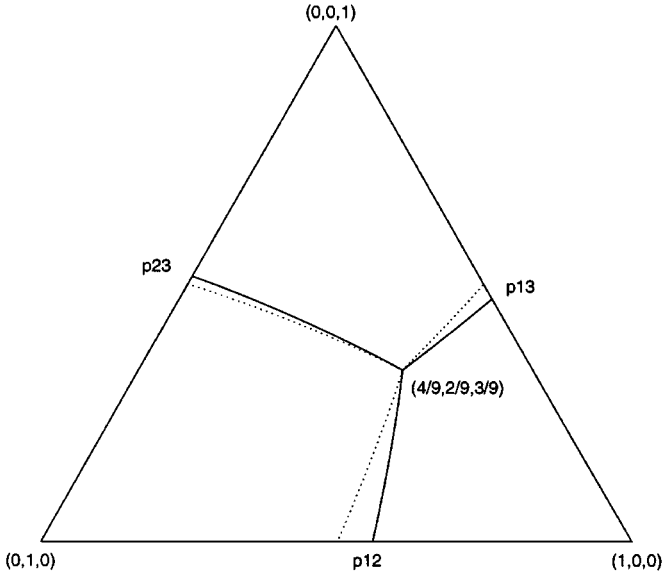

FIG. 19. The projection triangle for a 160–80–120 degree junction with (solid) and without (dotted) a constant component to the motion: $\mathbf{p}_{12} = (\frac{1}{2}+\frac{1}{2}e_{12}\sqrt{\frac{\Delta t}{2\pi}}, \frac{1}{2}-\frac{1}{2}e_{12}\sqrt{\frac{\Delta t}{2\pi}}, 0)$; $\mathbf{p}_{23} = (0, \frac{1}{2}+\frac{1}{2}e_{23}\sqrt{\frac{\Delta t}{2\pi}}, \frac{1}{2}-\frac{1}{2}e_{23}\sqrt{\frac{\Delta t}{2\pi}})$; $\mathbf{p}_{13} = (\frac{1}{2}+\frac{1}{2}e_{13}\sqrt{\frac{\Delta t}{2\pi}}, 0, \frac{1}{2}-\frac{1}{2}e_{13}\sqrt{\frac{\Delta t}{2\pi}})$.

2. Scale and rotate each curve defined by $\theta_{ij}(\cdot)$ according to

$$\tilde{\theta}_{ij}(r) = \theta_{ij}\left(\frac{r_0}{r_{\mathbf{p}_{ij}}} r\right) + \theta_{\mathbf{p}_{ij}} - \theta_{ij}(r_0), \tag{10}$$

where

$$\mathbf{p}_{ij} = \left(\frac{1}{2} + \frac{1}{2}e_{ij}\sqrt{\frac{\Delta t}{2\pi}}\right)\hat{e}_i + \left(\frac{1}{2} - \frac{1}{2}e_{ij}\sqrt{\frac{\Delta t}{2\pi}}\right)\hat{e}_j,$$

$$r_0 = \left\| \left(\frac{\theta_1}{2\pi}, \frac{\theta_2}{2\pi}, \frac{\theta_3}{2\pi}\right) - \frac{1}{2}(\hat{e}_i + \hat{e}_j) \right\|,$$

$$\hat{e}_i = \begin{cases} (1,0,0) & \text{if } i = 1 \\ (0,1,0) & \text{if } i = 2 \\ (0,0,1) & \text{if } i = 3 \end{cases}$$

and $(r_{\mathbf{p}_{ij}}, \theta_{\mathbf{p}_{ij}})$ are the polar coordinates of the point, $\mathbf{p}_{ij}$. This gives a simple expression for each branch of the desired projection triangle,

$$\left\{(r, \tilde{\theta}_{ij}(r)) : 0 \le r \le r_{\mathbf{p}_{ij}}\right\}.$$

Note that we have scaled r in the first term of Eq. (10) so that $\tilde{\theta}_{ij}(\cdot)$ is defined on the appropriate domain, $[0, r_{\mathbf{p}_{ij}}]$. The remaining two terms simply rotate each curve so that property (a) above is satisfied.

Combining this algorithm with that of the previous section gives a method for evolving junctions according to the multiphase model:

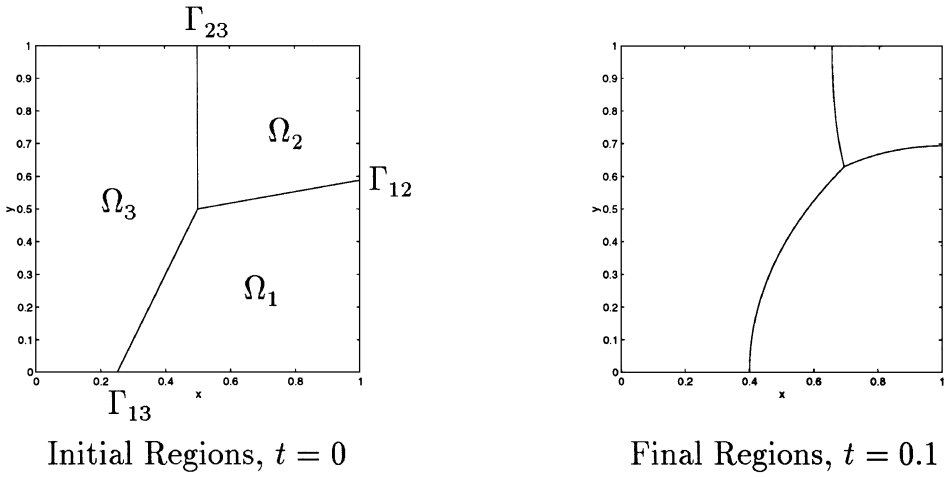

FIG. 20. A test problem for a 160–80–120 degree junction. Here, $(\gamma_{12}, \gamma_{23}, \gamma_{13}) = (\sin(\frac{8}{9}\pi), \sin(\frac{4}{9}\pi), \sin(\frac{2}{3}\pi))$ and $(e_{12}, e_{13}, e_{23}) = (-2, -\frac{1}{2}, \frac{3}{2})$.

MULTIPHASE MOTION ALGORITHM. Given an angle configuration $(\theta_1, \theta_2, \theta_3)$, coefficients $(\gamma_{12}, \gamma_{13}, \gamma_{23})$, and constants (e_{12}, e_{13}, e_{23}):

BEGIN
(1) Construct a projection triangle according to
the Projection Triangle Algorithm for Multiphase Motion.
(2) Carry out steps (2)–(5) of the Generalized Curvature Algorithm
using the projection triangle derived in step (1).
END

5.2. *Numerical Experiments*

We now apply the Multiphase Motion Algorithm to the case where each branch of a junction moves with a different normal velocity, $v_n = \gamma_{ij}\kappa + e_{ij}$.

For example, consider the evolution of the three phase problem given in Fig. 20. Using the Multiphase Motion Algorithm with $f = f_2$ (see Eq. (8)), the position of the triple point and the change in the area of Ω_1 were compared with the exact results (see Footnote 6) for several Δt. The results from a number of experiments are reported in Table V.

TABLE V
Results for a 160–80–120 Degree Junction

	Junction position		Phase area change for Ω_1	
Δt	*|Error|*	*Conv. rate*	*|Error|*	*Conv. rate*
0.01	6.82e-02	—	2.61e-02	—
0.005	4.64e-02	0.56	1.83e-02	0.51
0.0025	3.20e-02	0.54	1.29e-02	0.51
0.00125	2.22e-02	0.53	9.11e-03	0.50
0.000625	1.55e-02	0.52	6.43e-03	0.50
0.0003125	1.09e-02	0.51	4.56e-03	0.50

These results are suggestive of an $\mathcal{O}(\sqrt{\Delta t})$ error which is experimentally the same as that found for pure motion by curvature.

6. SHAPE CHANGES WITH MANY PHASE REGIONS

In the previous section, we described a method for evolving a three phase junction with a normal velocity, $v_n = \gamma_{ij}\kappa + e_{ij}$. To extend this method to r phase regions, we apply two additional considerations:

(1) For each point on the domain, the three largest U_i, $1 \le i \le r$, are sharpened according to the projection triangle for those components. All remaining components are set to zero during sharpening.

(2) The function f_n (see Eq. (8)) is extended to r phase regions:

$$f_n(\mathbf{U}) = \frac{\sum_{1\le i\le j\le r}\left(\mathbf{U}^{\gamma_{ij}}\Big/\left|\prod_{\substack{1\le k\le r\\ k\ne i,k\ne j}} U_k^{\gamma_{ij}}\right|^n\right)}{\sum_{l=1}^{r}\sum_{1\le i\le j\le r}\left(\mathbf{U}_l^{\gamma_{ij}}\Big/\left|\prod_{\substack{1\le k\le r\\ k\ne i,k\ne j}} U_k^{\gamma_{ij}}\right|^n\right)}.$$

Applying these modifications to the Multiphase Motion Algorithm gives a method for approximating the model (1) when many phase regions are present. We have found that the results from this method agree with the recent variational approach given in [18] even when topological mergings and breakings occur.

For example, consider the evolution of the four phase problem given in Fig. 21a. Using our diffusion-generated approach with $f = f_1$ and a step size of $\Delta t = 0.000125$, the interfaces were determined for several times, t (see Figs. 21b–21d). These results agree well with the variational approach (cf. Fig. 22).

Our new algorithm also naturally treats problems which involve the formation of junctions. Consider, for example, the evolution of the four regions given in Fig. 23a. Using our diffusion-generated approach with $f = f_1$ and a step size $\Delta t = 0.00025$, the interfaces were determined for several times, t. Here, we find that the interface between the regions Ω_1 and Ω_2 travels to the right to form two new junctions (see Fig. 23b). These triple points eventually move to the top and bottom of regions Ω_3 and Ω_4 as is shown in Figs. 23c and 23d. It is noteworthy that this example cannot be treated using the variational approach [18], since that method is inconsistent with the given values of γ_{ij}.

7. SUMMARY

In this work, we have presented a diffusion-generated approach for evolving multiple junctions according to the multiphase model (1). Our method naturally treats topological mergings and breakings, produces no overlapping regions or vacuums, and can be made very fast. We have also shown that our approach may be applied to an important class of problems which cannot be treated using other methods (see the previous section).

Asymptotic expansions were also given to explain why our method reproduces the correct junction angles (to within $\mathcal{O}(\sqrt{\Delta t})$) and numerical studies were provided to show that our approach agrees with front tracking [4] and a recent variational method [18] on a variety of simple problems.

Further work suggested by the results of this paper include a more detailed theoretical investigation of our method and an extension to the full range of possible model problems

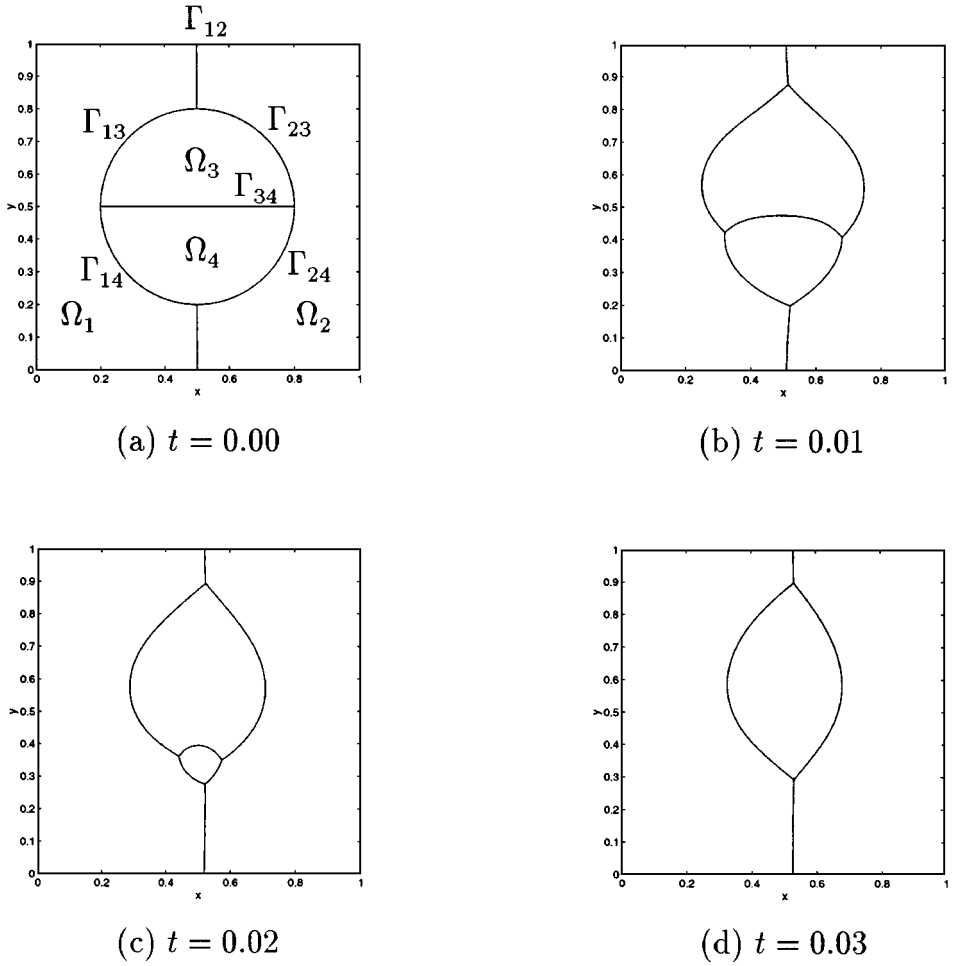

FIG. 21. A test problem at various times, t. Here $(\gamma_{12}, \gamma_{13}, \gamma_{14}, \gamma_{23}, \gamma_{24}, \gamma_{34}) = (\frac{5}{4}, \frac{3}{4}, \frac{5}{4}, 1, \frac{3}{2}, 1)$, $(e_{12}, e_{13}, e_{14}, e_{23}, e_{24}, e_{34}) = (-\frac{1}{2}, \frac{1}{2}, -\frac{3}{2}, 1, -1, -2)$ and all angles are prescribed by the classical condition (3).

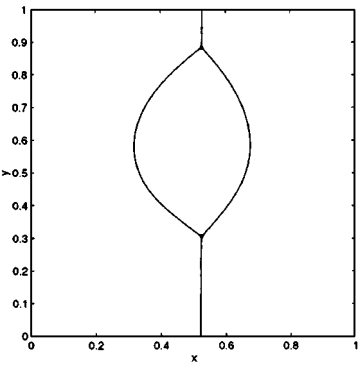

FIG. 22. The solution from the variational approach at $t = 0.03$.

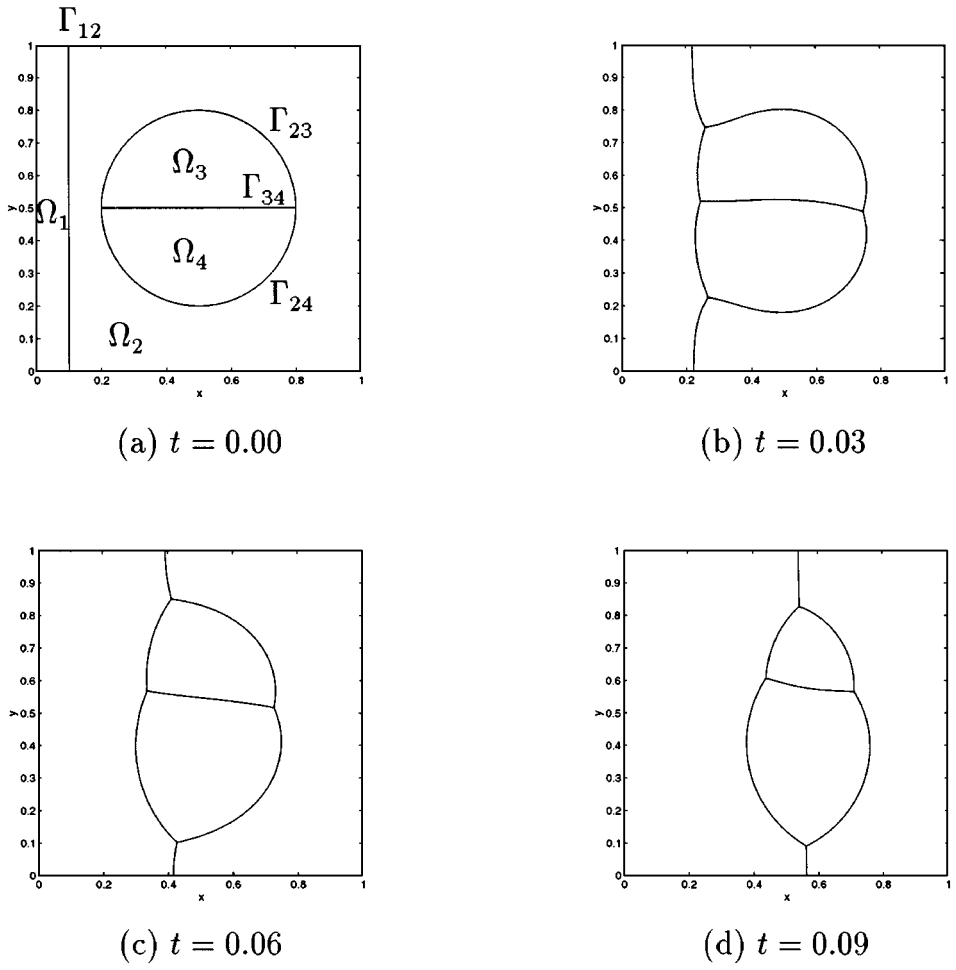

(a) $t = 0.00$ (b) $t = 0.03$

(c) $t = 0.06$ (d) $t = 0.09$

FIG. 23. A test problem at various times, t. Here $(\gamma_{12}, \gamma_{13}, \gamma_{14}, \gamma_{23}, \gamma_{24}, \gamma_{34}) = (1, 1, 1, \frac{\text{sqrt}(3)}{2}, 1, \frac{1}{2})$, $(e_{12}, e_{13}, e_{14}, e_{23}, e_{24}, e_{34}) = (-4, -1, 0, 3, 4, 1)$ and all angles are prescribed by the classical condition (3).

(currently, our approach cannot be applied if some γ_{ij} is sufficiently small; see subsection 4.2). Finally, extensions to anisotropic motions (e.g., [7]) and to constrained motions (e.g., [15]) would be of interest.

ACKNOWLEDGMENTS

I thank Barry Merriman and Stan Osher for helpful discussions. I also thank Brian Wetton and Hong-Kai Zhao for the use of their tracking and variational codes.

REFERENCES

1. S. Angenent and M. E. Gurtin, Multiphase thermodynamics with interfacial structure. 2. Evolution of an isothermal interface, *Arch. Rational Mech. Anal.* **108**, 323 (1989).
2. G. Barles and C. Georgelin, A simple proof of convergence for an approximation scheme for computing motions by mean curvature, *SIAM J. Numer. Anal.* **32**(2), 484 (1995).

3. L. Bronsard and F. Reitich, On three-phase boundary motion and the singular limit of a vector-valued Ginzburg–Landau equation, *Arch. Rational Mech. Anal.* **124**, 355 (1993).
4. L. Bronsard and B. T. R. Wetton, A numerical method for tracking curve networks moving with curvature motion, *J. Comput. Phys.* **120**(1), 66 (1995).
5. B. W. Char, K. O. Geddes, G. H. Gonnet, B. L. Leong, M. B. Monagan, and S. M. Watt, *Maple V Language Reference Manual* (Springer-Verlag, New York/Berlin, 1991).
6. L. C. Evans, Convergence of an algorithm for mean curvature motion, *Indiana Univ. Math. J.* **42**, 553 (1993).
7. H. Garcke, B. Nestler, and B. Stoth, On anisotropic order parameter models for multi-phase systems and their sharp interface limits, *Phys. D*, in press.
8. P. Mascarenhas, *Diffusion Generated Motion by Mean Curvature*, CAM Report 92-33, University of California, Los Angeles, 1992.
9. B. Merriman, J. Bence, and S. Osher, Diffusion generated motion by mean curvature, in *Computational Crystal Growers Workshop*, edited by J. E. Taylor (Amer. Math. Soc., Providence, RI, 1992), p. 73.
10. B. Merriman, J. Bence, and S. Osher, Motion of multiple junctions: A level set approach, *J. Comput. Phys.* **112**(2), 334 (1994).
11. F. Reitich and H. M. Soner, *Three-Phase Boundary Motions under Constant Velocities*. I. *The Vanishing Surface Tension Limit*, Technical Report 94-NA-015, Centre for Nonlinear Analysis, Carnegie Mellon University, 1994.
12. S. J. Ruuth, An algorithm for generating motion by mean curvature, in *Proceedings, 12th International Conference on Analysis and Optimization of Systems Images, Wavelets and PDE's, Paris, France, 1996*, p. 82.
13. S. J. Ruuth, *Efficient Algorithms for Diffusion-Generated Motion by Mean Curvature*, Ph.D. thesis, University of British Columbia, Vancouver, Canada, 1996.
14. S. J. Ruuth, *Efficient Algorithms for Diffusion-Generated Motion by Mean Curvature*, CAM Report 97-33, University of California, Los Angeles, 1997.
15. S. J. Ruuth, A diffusion-generated approach to a nonlocal, volume-preserving motion, *in Preparation*.
16. C. S. Smith, Grain shapes and other metallurgical applications to topology, in *Metal Interfaces* (American Society for Metals, Cleveland, 1952), p. 65.
17. J. E. Taylor, J. W. Cahn, and C. A. Handwerker, I-Geometric models of crystal growth, *Acta Metall. Meter.* **40**(7), 1443 (1992).
18. H. Zhao, T. Chan, B. Merriman, and S. Osher, A variational level set approach to multiphase motion, *J. Comput. Phys.* **127**, 179 (1996).